MINIREVIEW

Check for updates

A comprehensive analysis from the basics to the application of V-cathodes in Zn–V static and flow batteries

Yufei Li,† Jie Chen 🔟 † and Guanjie He 🔟 *

Electrochemical energy storage devices using zinc anodes and aqueous solutions have the characteristics of low cost, easy manufacture, and intrinsic safety. As an important part of modern aqueous batteries, zinc batteries have attracted extensive attention in the academic community. Among them, vanadium-based materials have been widely gaining attention as cathode materials in static aqueous zinc-ion batteries owing to their multiple valence states and abundant resources. In addition, zinc–vanadium flow batteries using the vanadium electrolyte for energy storage have also been gradually developed, which further expanded the application of vanadium-based materials in aqueous zinc batteries. In this review, an overview of zinc–vanadium batteries (including static batteries and flow batteries) is briefly discussed, including their working mechanism, classification, structure, existing problems, and improvement strategies, for promoting further development of this field.

1. Introduction

With the increasing demand for energy, continuous consumption of non-renewable energy sources and increasing environmental pollution, the development and energy storage of renewable energy sources, such as solar, wind and tidal power, are attracting significant attention.[1] Therefore, it is necessary to vigorously research and develop large-scale energy storage

Department of Chemistry, University College London, 20 Gordon Street, London, WC1H 0AJ, UK. E-mail: g.he@ucl.ac.uk

† Yufei Li and Jie Chen contribute to the work equally.

equipment. In recent years, traditional ion batteries, such as lithium-ion and sodium-ion batteries, have dominated the entire rechargeable battery market because of their mature large-scale manufacturing processes. Although lithium-ion and sodium-ion batteries are very successful in commercial sales, lithium-ion batteries have problems, such as safety and easy thermal runaway, and sodium-ion batteries offer relatively low energy density and poor cycling performance, which have limited the development of these two types of batteries and made them unsuitable for large-scale energy storage. On the contrary, the new zinc-ion battery is safe, cost-effective, and environmentally friendly, making it a strong competitor as a large-scale energy storage equipment.[1]

Yufei Li is currently an undergraduate student in the Department of Chemistry at University College London (UCL). She has done research on electrochemistry, macrocyclic compounds and synthesis of COF materials. Her research interests focus on electrocatalysis and battery materials in aqueous zinc-ion batteries.

Yufei Li

Jie Chen is currently a PhD student in the Department of Chemistry at University College London (UCL). He obtained his Bachelor's (2020) and Master's (2023) degrees in Physics from Lanzhou University and served as a visiting student at Fudan University. His research interests mainly focus on the interface between electrodes and electrolytes in zinc-ion batteries and interdisciplinary discussions between physics and electrochemistry.

Jie Chen

The research on modern static water zinc-ion batteries can be traced back to 2012; Kang *et al.* constructed a secondary aqueous zinc-ion battery based on an alpha-MnO_2 cathode and $ZnSO_4$ aqueous electrolyte and revealed the intercalation/extraction mechanism of Zn^{2+} ions.[2] Later in 2016, Nazar's team synthesized layered $Zn_{0.25}V_2O_5 \cdot nH_2O$ for the first time and used it as a cathode material for aqueous zinc-ion batteries. Its specific capacity reached 300 mA h g^{-1}, and the capacity retention rate was more than 80% after 1000 cycles, showing the huge application potential of vanadium oxide.[1] Since then, manganese oxide and vanadium oxide have become the most typical cathode materials for static aqueous zinc-ion batteries.

In addition to zinc-ion static batteries, Zn flow batteries can also address the problem of large-scale energy storage, and their potential advantages are greater than those of static batteries, because the power and capacity of flow batteries can be configured independently; the power is determined by the number of stacks, and the capacity is determined by the volume of the electrolyte.[3] This design makes them more flexible in large-scale and long-term energy storage scenarios. In the process of deep charging and discharging, the performance of flow batteries is more stable and suitable for long-term energy storage (more than 4 hours). At present, the commercial market circulates all-vanadium flow batteries and zinc–bromine flow batteries, but the development of these two flow batteries are limited owing to their low energy density and safety problems caused by electrolyte corrosion and growth of zinc dendrites. In 2012, the concept of Zn–V flow battery was first proposed, and V(IV)/V(V) and Zn^{2+}/Zn redox couples were assembled into a flow battery, which broadened the application of vanadium-based materials in aqueous zinc batteries.[3]

In this review, zinc–vanadium batteries are separated into static batteries and flow batteries, as shown in Fig. 1. We first describe the different energy storage mechanisms of these two batteries, then introduce the existing problems of vanadium-based zinc-ion batteries and Zn–V flow batteries, and finally put

forward some corresponding improvement strategies, and further prospect the future development.

2. Zn–V static batteries

2.1. Mechanisms

2.1.1. Zn^{2+} intercalation/extraction. Various open structures like tunnels and layers (*e.g.* V_2O_5, V_6O_{13} and VO_2), as shown in Fig. 2a–c, facilitate the reversible insertion and extraction of Zn^{2+}. During discharging, Zn^{2+} ions insert into the vanadium oxide structure. In some cases (*e.g.* V_6O_{13}), the Zn^{2+} ions insert into empty sites to form a new $Zn_{0.25}V_2O_5 \cdot H_2O$ phase. During charging, Zn^{2+} ions are extracted from the structure, and the newly formed phase disappears, as shown in Fig. 2d.[1]

In many studies, V_2O_5 has been used to explain the intercalation/extraction mechanism of Zn^{2+} ions because its layered structure and large laminar gap are conducive to the movement of Zn^{2+} ions, as shown in Fig. 2e, and it can attain a high theoretical capacity of 589 mA h g^{-1} for the whole charge–discharge process.[2] The redox reactions of vanadium ions occur during the insertion and extraction of Zn^{2+}. During discharging, Zn^{2+} ions embed between the layers of V_2O_5, and vanadium ions undergo reduction (V^{5+} to V^{4+} ions). As the concentration of intercalated Zn^{2+} ions increases, part of V^{4+} ions will continue to reduce to V^{3+} ions. During charging, an oxidation reaction occurs (V^{3+} to V^{4+} or V^{5+} ions), and the V_2O_5 structure detaches from the Zn^{2+} ions.[3] The structural distortion of V_2O_5 due to the intercalation of Zn^{2+} ions will revert to the structure after the removal of Zn^{2+} ions, which is proven by the remained crystal structure and phase transition of the battery material.[2] Therefore, the Zn^{2+} intercalation/extraction reaction is reversible, and the battery can continuously charge and discharge. In addition, the high structural stability of the cathode material makes the cycle life of the battery long.

2.1.2. H^+/Zn^{2+} co-intercalation/extraction. The H^+/Zn^{2+} co-intercalation/extraction mechanism occurs in electrolytes containing low concentrations of zinc ions or slightly acidic ones. In acidic electrolytes, H^+ in the solution participate in the reaction mechanism. Vanadium ions have the highest oxidation state at the start of the co-insertion process. The process of zinc ion insertion is the same as in the Zn^{2+} insertion/extraction mechanism. Simultaneously, H^+ ions also intercalate into the vanadium oxide lattice. The hydrogen ions can originate from the electrolyte or from the water molecules present in the system. The insertion of H^+ ions helps to balance the charge and stabilize the structure during the insertion of Zn^{2+} ions. Along with Zn^{2+}, hydrogen ions (H^+) are also deintercalated from the lattice. The small size and monovalent charge minimize lattice strain and structural degradation, acting as "pillars". These also enable more insertions of ions, accessing confined sites unreachable by Zn^{2+}.[7] This extraction process involves the oxidation of vanadium ions back to their higher oxidation state, such as V^{5+}, to facilitate the release of both Zn^{2+} and H^+ ions, as shown in Fig. 3d.[7] In 2020, Zhu *et al.* reported a series of experimental and calculation results that further
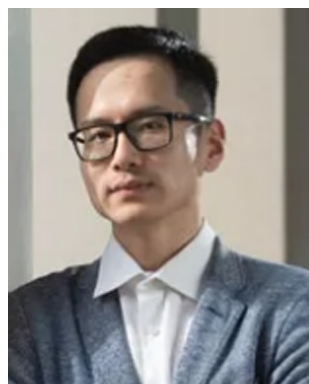
Guanjie He is an Associate Professor in the Department of Chemistry at University College London (UCL). He received his PhD degree from UCL in 2018 and visited Yale University during his PhD study. He has worked at Queen Mary University of London and the University of Lincoln. His research fields are mainly aqueous batteries, electrocatalytic materials and devices, advanced characterization, and simulation. He has received the EPSRC New Investigator Award, ERC Starting Grant and STFC Early Career Awards for his research on zinc-ion batteries.
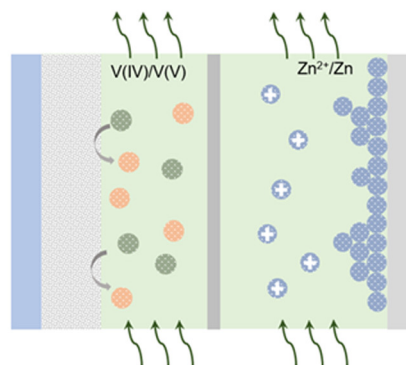
Guanjie He
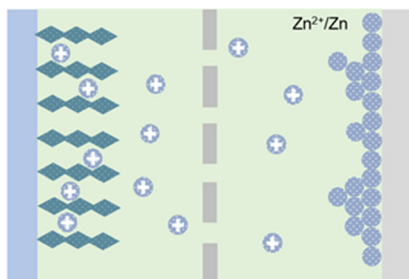
Fig. 1 Schematic of the static Zn–V battery (vanadium-based zinc-ion batteries) and Zn–V flow battery.
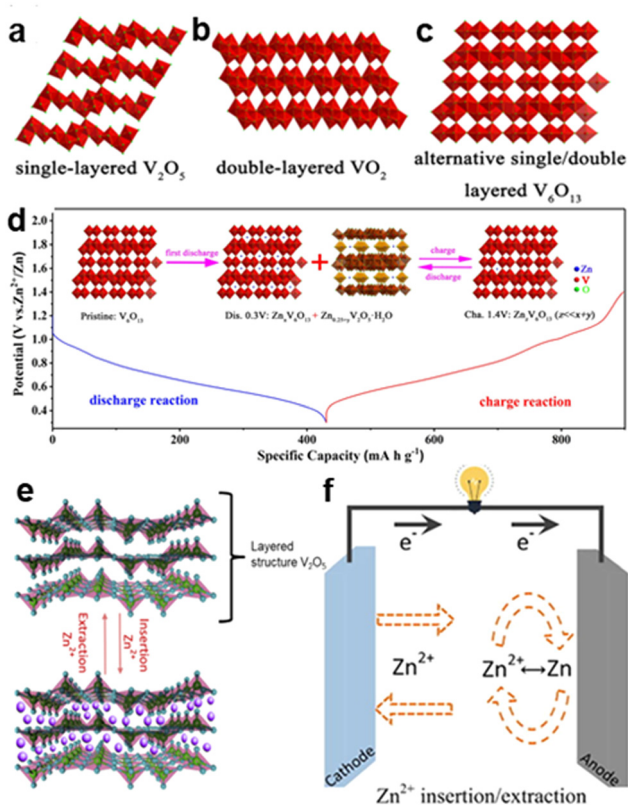

Fig. 2 Schematic of (a)–(c) Structures of common vanadium oxides with the Zn^{2+} intercalation/extraction mechanism. (d) Zn^{2+} intercalation/extraction mechanism of V_6O_{13}.[4] Copyright 2019, Wiley-VCH GmbH. (e) Zn^{2+} intercalation/extraction mechanism of V_2O_5.[5] Copyright 2020, Elsevier. (f) General Zn^{2+} intercalation/extraction mechanism in static Zn–V batteries (vanadium-based zinc-ion batteries).[6] Copyright 2021, Elsevier.

Fig. 3 Schematic of (a) Structure of H–VO$_2$. (b) Possible sites in H–VO$_2$ for H^+/Zn^{2+} co-intercalation/extraction. (c) Migration pathways for H^+ (left) and Zn^{2+} (right) ions in H–VO$_2$.[8] Copyright 2020, Elsevier. (d) H^+/Zn^{2+} co-intercalation/extraction mechanism in static Zn–V batteries (vanadium-based zinc-ion batteries).[6] Copyright 2021, Elsevier.

demonstrated the H^+/Zn^{2+} co-intercalation/extraction mechanism occurring in H–VO$_2$, as shown in Fig. 3a–c. The results show that H^+ intercalation is dominant in the early stage of discharge, while H^+/Zn^{2+} intercalation is dominant in the late stage of discharge.[8] Because the charge valence and capacity of H^+ are smaller than those of Zn^{2+}, they have a higher diffusion kinetics. This mechanism works in scenarios with high specific
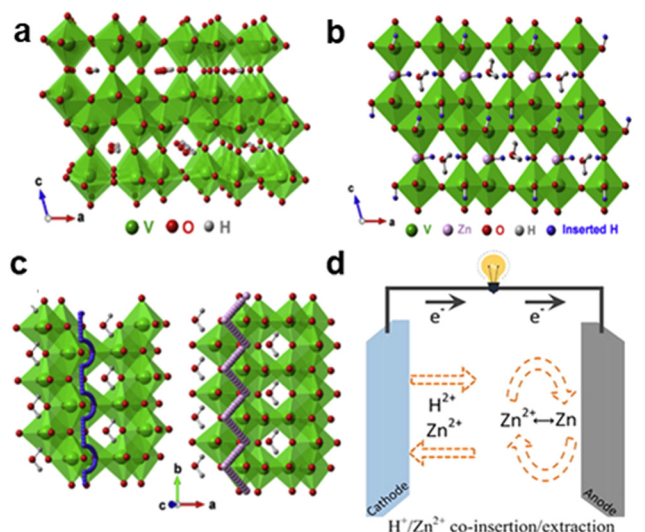
capacity, but may lead to structural instability, such as structural collapse, due to the change of the crystal structure during the phase transition of VO$_2$.[9]

2.1.3. H$_2$O/Zn^{2+} intercalation/extraction. The H_2O/Zn^{2+} intercalation/extraction is similar to the intercalation and extraction processes in the H^+/Zn^{2+} mechanism, but the H^+ insertion/extraction is replaced by the water molecule insertion/extraction. Comparing these two mechanisms, the contribution of H^+ ions to the overall capacity is limited in the H^+/Zn^{2+} mechanism, and its high mobility can sometimes lead to structural distortions or instability over time.[1] Water molecules from the aqueous electrolyte co-intercalate into the vanadium oxide lattice. These water molecules function as structural pillars, enlarging the channel dimensions and enhancing the capacity and rate capability during discharging. In 2016, Kundu *et al.* reported a novel cathode material (Zn$_{0.25}$V$_2$O$_5$·nH$_2$O) to

achieve a rapidly reversible H_2O/Zn^{2+} intercalation/extraction mechanism.[1,10] The high charge density of Zn^{2+} ions can be buffered by the structured water, which also minimises the activation energy of the cathode material's interfacial charge transfer, speeds up the ion diffusion kinetics during the intercalation and extraction of Zn^{2+} ions, and realises the self-lubricating effect of ion transport. Additionally, the structured water can reversibly expand and contract the layer spacing of $Zn_{0.25}V_2O_5$, which is useful for Zn^{2+} intercalation and extraction.[10] During the charge–discharge cycles of zinc-ion batteries, Zn^{2+} ions undergo reversible insertion and extraction within the cathode, while water molecules become integrated into the cathode's structural framework, as shown in Fig. 4a. This dual mechanism enables the battery to achieve an impressive energy density (450 W h L^{-1}) and sustain a capacity retention rate exceeding 80% over 1000 cycles, as shown in Fig. 4b and c.[1] In addition to the above-mentioned ZnVO, the cathode materials that demonstrate this mechanism also include $V_2O_5{\cdot}nH_2O$, $V_6O_{13}{\cdot}nH_2O$ and $NaV_3O_8{\cdot}xH_2O$. These materials illustrate how the presence of crystallization water in layered structures not only enhances ion transport by reducing diffusion barriers for the divalent Zn^{2+} ions but also stabilizes the framework during repeated charge/discharge cycles.[11] Notably, the zinc anode remains free of dendrite formation, a critical advantage that enhances both safety and long-term stability.

2.1.4. Chemical conversion. Chemical conversion reactions occur in vanadium-based cathode materials, meaning that during the initial charge/discharge cycles, the materials' chemical composition and structure undergo substantial changes (an irreversible phase transformation). The transformation of vanadium oxide (e.g., V_2O_5, VO_2, V_2O_3) results in a new stable phase that enables prolonged Zn^{2+} storage, as shown in Fig. 5a. This
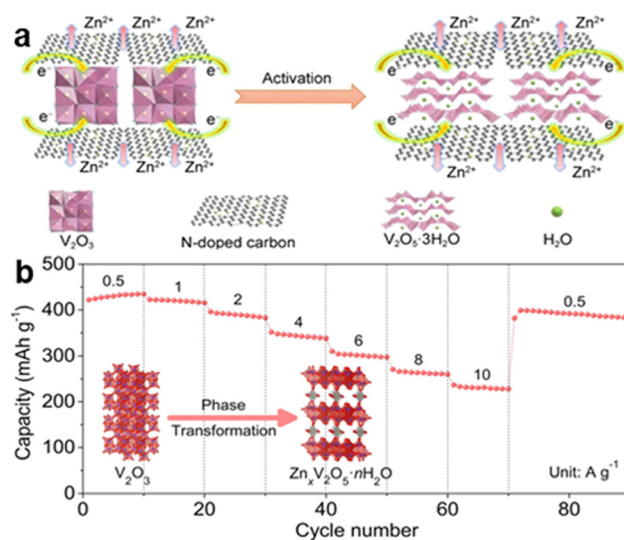

Fig. 4 Schematic of (a) H_2O/Zn^{2+} co-intercalation/extraction mechanism of $Zn_{0.25}V_2O_5{\cdot}nH_2O$ in static Zn–V batteries (vanadium-based zinc-ion batteries). (b) Energy density value of $Zn_{0.25}V_2O_5{\cdot}nH_2O$ compared with two other known materials for AZIBs. (c) Extended cycling performance and the corresponding coulombic efficiency at an 8C rate showing a capacity retention rate exceeding 80% over 1000 cycles.[1] Copyright 2016, Nature Energy.

Fig. 5 Schematic of (a) Chemical conversion mechanism of V_2O_3.[16] Copyright 2023, Springer Nature Limited. (b) Phase transition from V_2O_3 to $Zn_xV_2O_5{\cdot}nH_2O$ in static Zn–V batteries (vanadium-based zinc-ion batteries).[13] Copyright 2021, Elsevier.

transformation stabilizes after a few cycles, enhancing long-term Zn^{2+} storage.[10] Notable examples include V_2O_3@C, which transitions into a hydrated $Zn_xV_2O_5{\cdot}nH_2O$ structure with improved cycling stability, as shown in Fig. 5b, and VO_2-Graphene (VO_2-rG), which converts into $V_2O_5{\cdot}nH_2O$ with enhanced Zn^{2+} diffusion pathways.[12,13] Additionally, vanadium oxynitride (VN_xO_y) cathodes exhibit both cation ($V^{3+} \leftrightarrow V^{2+}$) and anion ($N^{3-} \leftrightarrow N^{2-}$) redox reactions, providing high-rate capability and long cycle life.[9,14] $Zn_{0.3}V_2O_5{\cdot}1.5H_2O$ undergoes conversion into a porous layered Zn-rich vanadate, ensuring abundant active sites for Zn^{2+} storage.[15] The primary advantages of this mechanism include increased structural stability by preventing vanadium dissolution, enhanced Zn^{2+} storage capacity through multiple intercalation sites, and improved cycle life with minimal capacity decay. Overall, the conversion mechanism plays a crucial role in stabilizing vanadium-based cathodes, thereby enabling high-performance and long-lasting AZIBs.

2.1.5. Other types. The substitution/interaction reaction mechanism involves the replacement of pre-inserted metal ions (such as Na^+, K^+, or Mg^{2+}) with Zn^{2+} during cycling, improving structural stability and electrochemical performance. First proposed by Shan et al., this mechanism differs from conventional intercalation by enabling Zn^{2+} insertion at two distinct positions within the structure, allowing multi-electron charge transfer and significantly enhancing theoretical capacity.[17] In the $Ag_{0.4}V_2O_5/Zn$ battery system, Ag^+ is substituted by Zn^{2+} during discharging, resulting in three main phases: $Zn_xAg_{0.4}$-V_2O_5, $Zn_{2+x}(V_3O_8)_2$, and metallic Ag^0. Upon charging, the material reverts to $Ag_{0.4}V_2O_5$ and Ag^0, as shown in Fig. 6a. The in situ generated Ag^0 matrix provides high conductivity, enabling superior rate performance and stable cycling even at high current densities (e.g., 20 A g^{-1}).[18,19]
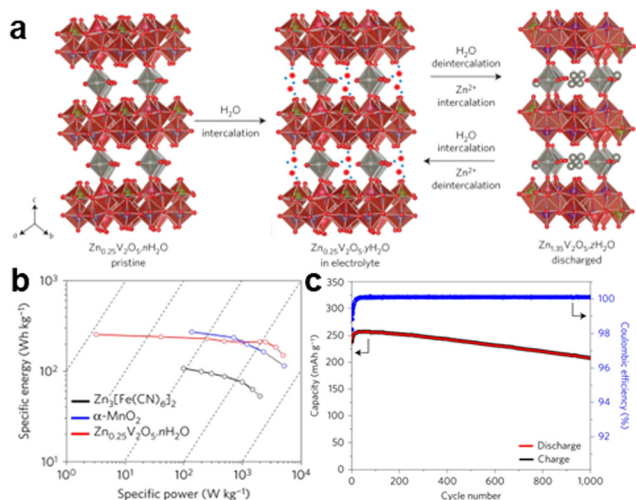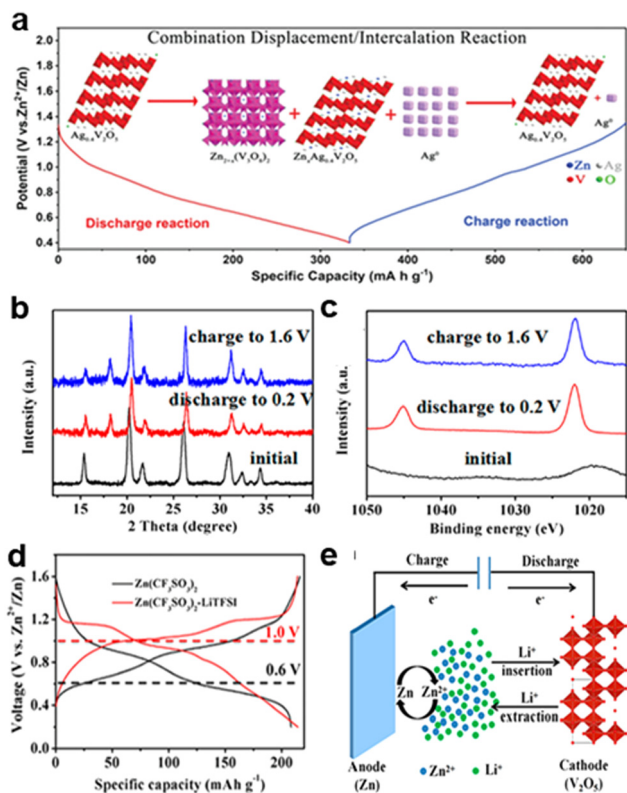
Fig. 6 Schematic of (a) Combination substitution/interaction reaction mechanism of $Ag_{0.4}V_2O_5$ during discharging/charging processes.[19] Copyright 2020, Wiley-VCH GmbH. (b) *Ex situ* XRD patterns collected in the Zn$(CF_3SO_3)_2$ electrolyte (black: initial state, red: discharged to 0.2 V; and blue: charged to 1.6 V) at 100 mA g^{-1}. (c) *Ex situ* XPS collected in the Zn$(CF_3SO_3)_2$–LiTFSI electrolyte at 100 mA g^{-1}. (d) Higher voltage platform of Zn/V_2O_5 batteries at 100 mA g^{-1}. (e) Hybrid metal ion mechanism.[20] Copyright 2017, the American Chemical Society.

The mixed metal ion mechanism involves the simultaneous participation of multiple cations, such as Zn^{2+} and Li^+, in the charge storage process. In the Zn/V_2O_5 hybrid-ion battery system, the use of a "water-in-salt" electrolyte (Zn $(CF_3SO_3)_2$–LiTFSI) enables both Zn^{2+} and Li^+ to intercalate into the V_2O_5 cathode during discharging, as shown in Fig. 6e. *Ex situ* XRD and XPS analyses confirm that Zn^{2+} primarily intercalates into V_2O_5, while Li^+ enhances structural stability by acting as an interlayer pillar, preventing structural collapse, and improving cycle life, as shown in Fig. 6b and c. This dual-ion interaction leads to a higher voltage platform, enhanced rate capability, and superior cycling stability compared to conventional single-ion Zn^{2+} intercalation, as shown in Fig. 6d and e. The hybrid system demonstrates high-capacity retention (80% after 2000 cycles at 2000 mA g^{-1}), highlighting its potential for high-performance energy storage.[20]

2.2. Classification and structures

2.2.1. Vanadium oxide. A variety of paths for Zn^{2+} ion intercalation and extraction are provided by vanadium oxides, which are potential cathode materials for aqueous zinc-ion batteries (AZIBs) due to their open frameworks and diverse oxidation states. V_2O_5 adopts a layered structure composed of $[VO_5]$ square pyramidal units linked by shared edges or vertices, forming sheets held together by weak vanadium–oxygen bonds, van der Waals forces, and hydrogen bonds, with an interlayer spacing of ~0.58 nm, as shown in Fig. 7a.[21] This layered design facilitates Zn^{2+} insertion but may suffer from structural instability. VO_2, with its d^1 electronic configuration, exhibits multiple polymorphs (A, B, D, M, R, and P), among which VO_2 (B), (D), and (M) are notable for AZIB applications, as shown in Fig. 7b–e.[22] VO_2 (B) features a tunnel-like framework of distorted $[VO_6]$ octahedrons sharing edges and corners, creating spacious channels for rapid Zn^{2+} diffusion.[3] VO_2 (D) has an orthorhombic structure with hexagonal close-packed vanadium ions, offering high electrical conductivity and ion accessibility in its metallic phase. VO_2 (M) forms a dense network of twisted $[VO_6]$ octahedrons, generating narrow tunnels (~0.318 nm) that optimize ion migration efficiency.[22] V_2O_3 possesses a three-dimensional tunnel structure where V^{3+} ions coordinate with six O^{2-} ions in edge-sharing $[VO_6]$ octahedra, ensuring structural robustness and efficient cation intercalation, as shown in Fig. 7f. Its enhanced electronic conductivity arises from delocalized 3d electrons along V–V bonds, outperforming many oxides.[11] Faster Zn^{2+} diffusion is favored by the tunnel-structured vanadium oxides compared to layered structures because of the larger spacing of the tunnel-structure. The movements of Zn^{2+} ions are less hindered, resulting in faster ion transport kinetics.[3] The layered architecture of V_2O_5 balances high capacity with challenges like aqueous dissolution, while VO_2 (B)'s open tunnels prioritize ion mobility but require stabilization against phase transitions. VO_2 (D)'s conductivity suits high-rate applications, and VO_2 (M)'s compact structure maximizes space utilization for ion kinetics. V_2O_3's 3D tunnels and inherent conductivity enhance cycling stability and rate performance.[22]

To compare battery performance among different materials and before and after improvements in the same material, either diffusion coefficient or kinetics is discussed. VO_2 exhibits a significantly higher diffusion coefficient (~$10^{-6.5}$ cm^2 s^{-1}) than most layered vanadium oxides such as MnVO and VOH
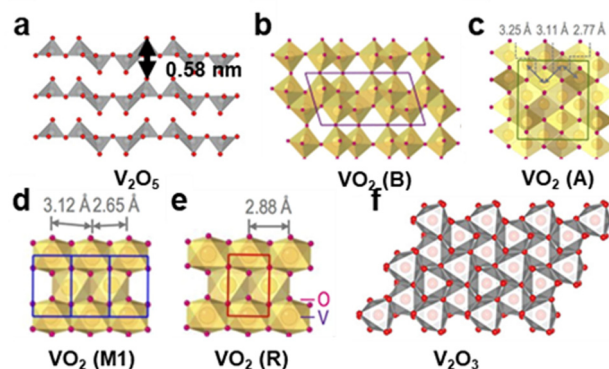

Fig. 7 Schematic of (a) and (f) Structures of V_2O_5 and V_2O_3.[22] Copyright 2016, Nature. (b)–(e) Structures of VO_2 (B, A, M1, and R).[23] Copyright 2020, Wiley-VCH GmbH.

($\sim 10^{-13}$ cm^2 s^{-1}), suggesting a lower migration energy barrier that facilitates faster charging/discharging and higher power density. This indicates that VO_2 nanorods represent a more promising cathode material for achieving superior battery performance.[24,25] Additionally, material modifications such as Mn ion intercalation and the creation of oxygen vacancies significantly enhance the battery performance by improving reaction kinetics and energy density. Specifically, Mn ion intercalation reduces charge transfer resistance, as evidenced by $V_2O_5 \cdot nH_2O$'s CV b-values shifting from 0.65, 0.76, 0.81, and 0.73 to 0.65, 0.86, 0.81, and 0.84, respectively.[26] In parallel, the introduction of oxygen vacancies lowers diffusion barriers and is applied to modify HVO. The modified HVO (T-HVO) shows improved b-values—approximately 0.90 and 0.89 compared to the 0.74 and 0.83 for unmodified HVO—indicating a transition to surface-controlled processes.[27] These changes lead to enhanced rate performance and faster charge/discharge capabilities.

2.2.2. Vanadium sulphide. For aqueous zinc-ion batteries (AZIBs), vanadium sulphides (VS_x) due to their unique structures and excellent electrochemical properties show promise as cathode materials. These materials exhibit diverse crystal structures, including layered (VS_2), chain-like (VS_4), and tunnel structures (V_5S_8), which are determined by the variable valence states of vanadium (V^{2+}, V^{3+}, V^{4+}, and V^{5+}) and its ability to form compounds with sulphur. VS_2 features a layered hexagonal structure with 5.76 Å interlayer spacing, enabling fast Zn^{2+} intercalation and high conductivity, as shown in Fig. 8a.[28] The broad spacing in the layers of VS_2 facilitates the

straightforward incorporation or removal of Li$^+$, Na$^+$, Zn^{2+}, or their solvated counterparts within the electrolyte.[11] However, it suffers from volume expansion and structural degradation during cycling. VS_4, on the other hand, has a quasi-1D chain structure with $[VS_4]^{2-}$ tetrahedral units and S_2^{2-} dimer groups, providing high theoretical capacity and structural flexibility, though it has limited electrical conductivity. Vanadium is in the same oxidation state in VS_2 and VS_4, but sulphide is in a different state (S_2^{2-} dimer in VS_4 and S^{2-} monomer in VS_2). Mixed vanadium sulphides, such as V_3S_4, V_5S_8, and V_2S_3, offer balance between conductivity and stability, delivering moderate capacity with improved cycling performance.[29]

In recent studies, He *et al.* reported that VS_2 nanosheets achieve high capacity (190.3 mA h g^{-1} at 0.05 A g^{-1}) and demonstrate stable cycling performance, as shown in Fig. 8c and d.[30] In comparison to VS_2, the VS_4@rGO cathode shows impressive capacity of 450 mA h g^{-1} at 0.5 A g^{-1}, attributed to the unique crystal structure of VS_4 and excellent conductivity of rGO, with capacity retention of 82% over 3500 cycles.[31]

2.2.3. Vanadium phosphates. Vanadium phosphates are a class of materials with unique structural and electrochemical properties that make them promising candidates for use as cathodes in aqueous zinc-ion batteries (AZIBs). These compounds typically exhibit layered or NASICON-type structures, which provide stable frameworks for ion transport. For example, vanadium phosphate ($VOPO_4$) has a layered structure that allows for efficient intercalation and deintercalation of Zn^{2+} ions. Under different specific conditions, layered vanadium phosphate can form three phases ($\alpha1$, $\alpha2$ and β phases), as shown in Fig. 9a–c. Both the $\alpha1$ and $\alpha2$ phases are connected to the PO_4 tetrahedron by a long V–O bond by a VO_6 octahedron shared by an angle, but vanadium is located in the equatorial plane on the same side as phosphorus in the $\alpha1$ phase, while vanadium is located on the opposite side to phosphorus in the $\alpha2$ phase. The β phase has a three-dimensional network structure that is connected in all directions by POV interactions. Although the ionic diffusion of the β phase is not as clear as that of the α phase, its structure still contributes, and the presence of high-valence vanadium (*e.g.*, V^{5+}) in these materials also contributes to their high theoretical capacity and discharge voltage plateau. However, challenges such as poor intrinsic conductivity and structural degradation during cycling need to be addressed to enhance their performance.[11]

As cathodes in aqueous zinc-ion batteries, vanadium phosphates can support multi-electron redox reactions, which significantly enhance their energy storage capabilities. The layered structure of $VOPO_4$ facilitates the intercalation of Zn^{2+} ions, enabling high specific capacity. For example, a new cathode material, potassium vanadyl phosphate ($KVOPO_4$), has been created by incorporating K$^+$ ions into the layers of $VOPO_4$, as shown in Fig. 9e. This approach not only maintains the stability of the crystal structure but also improves the diffusion kinetics of Zn^{2+} ions, leading to enhanced cycling stability and rate performance. The $KVOPO_4$ cathode exhibits significant reversible capacity of 153.2 mA h g^{-1} after 400 cycles at a current rate of 1 A g^{-1} and exhibits excellent rate performance with
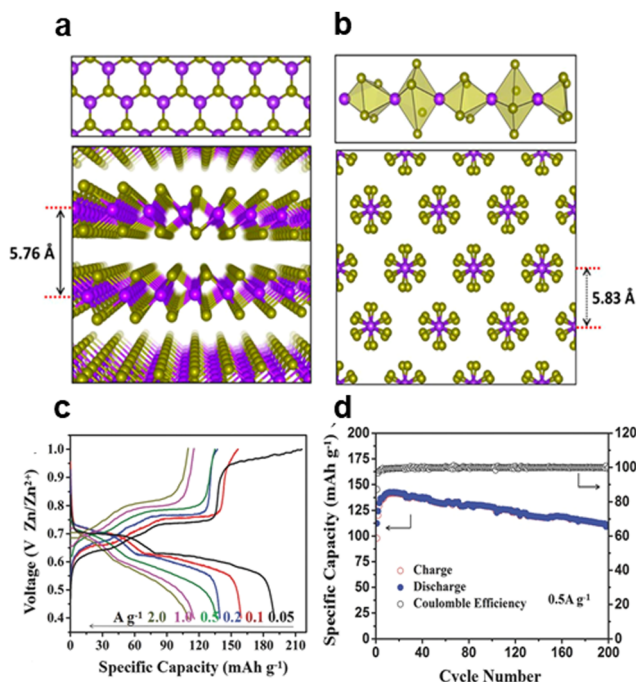

Fig. 8 Schematic structure of (a) VS_2 and (b) VS_4. The purple balls are V atoms, and the yellow balls are S atoms.[29] Copyright 2013, the American Chemical Society. (c) Charge and discharge curves of VS_2 at a current density from 0.05 to 2.0 A g^{-1}. (d) Long-term cycling properties of VS_2 at a current density of 0.5 A g^{-1}.[30] Copyright 2017, Wiley-VCH GmbH.
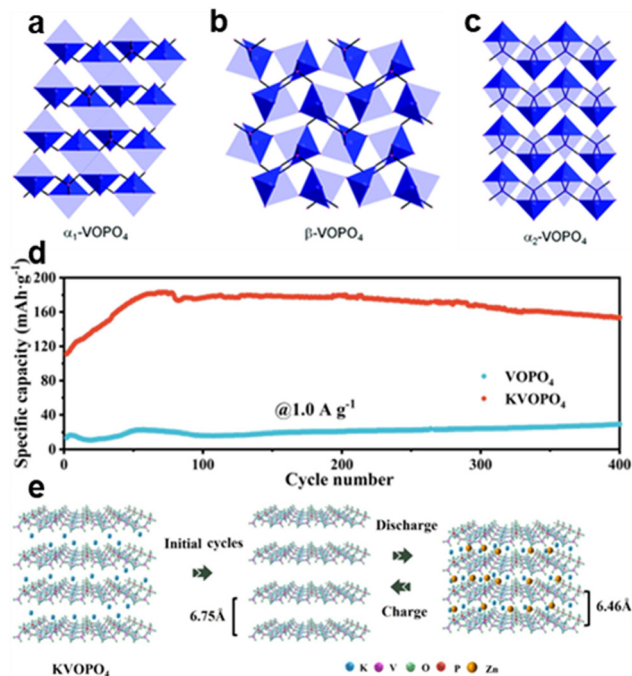
Fig. 9 Schematic of (a)–(c) Structures of vanadium phosphates in α1, α2 and β phases.[32] Copyright 2013, the Royal Society of Chemistry. (d) Reversible capacity of the VOPO$_4$ and KVOPO$_4$ electrodes at 1 A g^{-1}. (e) Zn-storage mechanism of the KVOPO$_4$ electrode during the cycling process.[33] Copyright 2024, Elsevier.

Fig. 10 Schematic of (a) Al-VN structure.[34] Copyright 2025, Elsevier. (b) Structure of VN/NC hybrid nanosheets.[35] Copyright 2022, the Royal Society of Chemistry. (c) Corresponding pore size distributions of VN/N-CNF compared with VN/N-MCNF showing the mesoporous structure. (d) Specific capacity of VN/N-CNF (242 mA h g^{-1} at 0.1 A g^{-1}) shown by rate performance.[36] Copyright 2025, European Chemical Societies.

119.4 mA h g^{-1} at 5.0 A g^{-1}, as shown in Fig. 9d.[33] This indicates that vanadium phosphates, due to their distinct structural characteristics and adjustable properties, can serve effectively as cathodes in aqueous zinc-ion batteries (AZIBs), offering high capacity, stability, and rate performance.

2.2.4. Vanadium nitrides. Vanadium nitrides (VNs) exhibit diverse structural configurations and tailored properties that make them highly effective cathode materials for aqueous zinc-ion batteries (AZIBs). Vanadium nitrides can form VN, V$_2$N and V$_3$N, and VN is also an isomer of VC and VO and has a face-centred cubic structure.[11] The specific structure of VN is determined by the method and conditions of their synthesis. Their crystal structures, such as cubic, layered, or porous frameworks, enable efficient Zn^{2+} ion diffusion and electronic conductivity. The strong covalent V–N bonding in VNs enhances structural stability against repeated cycling in aqueous electrolytes, while their metallic-like conductivity minimizes polarization losses. For example, cubic-phase vanadium nitride (VN) nanowires with a three-dimensional interconnected network achieve high capacity (544 mA h g^{-1} at 1 A g^{-1}), attributed to their open framework that facilitates rapid ion transport, as shown in Fig. 10a.[34] Similarly, layered VN nanosheets, with expanded interlayer spacing (e.g., ~0.45 nm), demonstrate improved Zn^{2+} storage kinetics, delivering 131 mA h g^{-1} at 10 A g^{-1} and retaining 85% capacity after 1000 cycles, as shown in Fig. 10b.[35] Additionally, porous VN composites, such as VN anchored on carbon nanofibers (VN/N-MCNF), leverage their mesoporous structure to enhance electrolyte accessibility and specific capacity, achieving
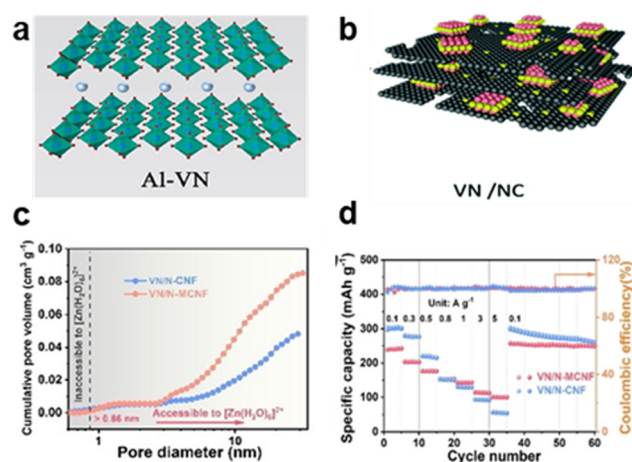
242 mA h g^{-1} at 0.1 A g^{-1}, as shown in Fig. 10e and f.[36] Vanadium nitrides are further modified by combining with rGO, which has high conductivity. The synthesised VN@rGO has specific capacity of 267.0 mA h g^{-1} at 1 A g^{-1}, and a specific capacity retention rate of 94.68% after 585 cycles.[37] These structural and electronic advantages position VNs as robust, high-capacity cathodes for durable AZIBs.[11,35]

2.2.5. Vanadates. Vanadates refer to a class of compounds containing vanadium in its highest oxidation state (+5), typically forming oxo anion structures. The simplest vanadate ion is the tetrahedral orthovanadate ion (VO$_4^{3-}$), which is commonly found in strong alkaline solutions of vanadium pentoxide (V$_2$O$_5$) and in the crystal structures of vanadate salts. Vanadates can exist in various forms, including VO$_4^{3-}$, V$_2$O$_7^{4-}$, V$_3$O$_9^{3-}$ and V$_{10}$O$_{28}^{6-}$.[38] These structures can form different crystal arrangements (layered or tunneled) depending on the counterions and environmental conditions. The layered or tunnel structure of vanadates provides a fast channel for the diffusion of Zn^{2+}. For example, zinc vanadate (Zn$_3$V$_2$O$_7$(OH)$_2$·2H$_2$O) features a layered structure with pillared Zn^{2+} ions and V$_2$O$_7^{4-}$ chains, enabling high capacity (135 mA h g^{-1} at 80 A g^{-1}) and high cycling stability (88% retention over 10 000 cycles) due to its expanded interlayer spacing (0.29 nm) and strong hydrogen-bonding network, as shown in Fig. 11a and b.[39] Sodium vanadate (NaV$_3$O$_8$·nH$_2$O) adopts a tunnel structure composed of VO$_6$ octahedra and VO$_5$ trigonal bipyramids, offering rapid ion diffusion kinetics of 410 mA h g^{-1} at 0.1 A g^{-1}, as shown in Fig. 11c and d.[7]

Vanadates are stable in alkaline and neutral environments but can undergo reduction in acidic conditions. In low pH solutions, vanadium can reduce to lower oxidation states. Vanadates exhibit excellent electrochemical properties due to the multiple oxidation states of vanadium (V^{5+}/V^{4+}). This allows them to undergo reversible redox reactions, making them
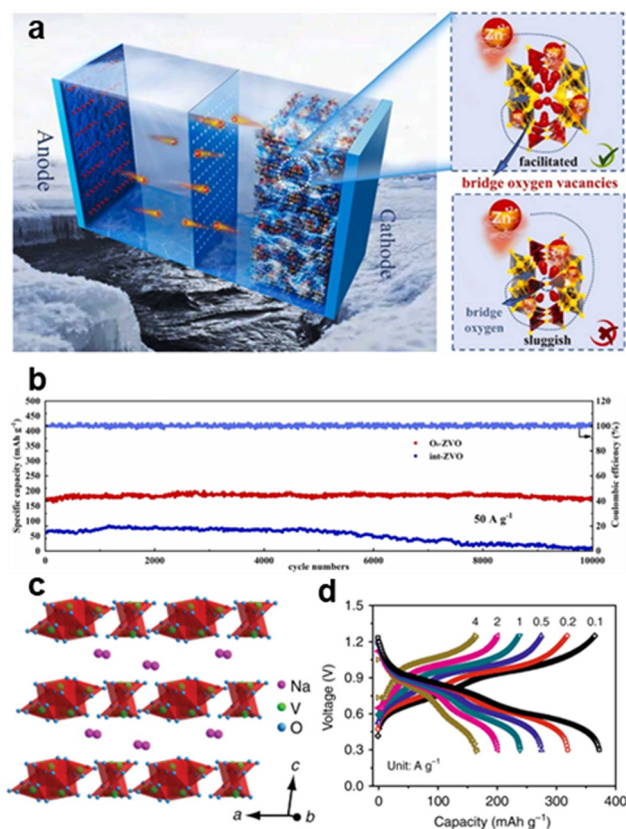
Fig. 11 Schematic diagram of (a) ZVO applied in a zinc-ion battery. (b) High cycling stability (88% retention over 10 000 cycles) compared with long cycle stability of O8–ZVO and int–ZVO at 50 A g^{-1}.[40] Copyright 2023, Elsevier. (c) Crystal structure of NaV$_3$O$_8$·nH$_2$O; Na$^+$ exists in the form of hydrated ions. (d) Rate performance of NVO electrodes in ZnSO$_4$/Na$_2$SO$_4$ electrolyte showing 410 mA h g^{-1} at 0.1 A g^{-1}.[7] Copyright 2018, Nature Communications.

suitable for energy storage applications.[38] Vanadates are extensively researched as cathode materials for AZIBs because of their high theoretical capacity, excellent cycling stability, and outstanding electrochemical characteristics. Materials like NaVO$_3$ and CaVO$_3$ have demonstrated encouraging outcomes regarding energy density and power density.[41,42]

2.3. Problems

2.3.1. Poor conductivity. The poor conductivity of vanadium-based cathode materials (e.g. V$_2$O$_5$ and VO$_2$) hampers the movement of charger carriers between the cathode material and electrolytes and leads to poor cycling stability due to the accumulation of charge and stress within the material.[43] Mechanisms leading to poor conductivity involve intrinsic material properties and electrostatic interactions. The low intrinsic conductivity of the bulk material is a consequence of the low electron concentration in the valence band and limited electronic transition likelihood near the Fermi level of vanadium oxides.[44] The layered or tunnel structures of vanadium oxides (e.g. V$_2$O$_5$) provide pathways for ion diffusion but do not inherently support efficient electron transport. The strong electrostatic attraction between Zn^{2+} ions and the V–O framework

in vanadium oxides elevate the energy barrier for ion diffusion. This not only hampers ion transport but also impacts the overall kinetics of electron transfer.[43]

2.3.2. Poor structural stability (V-dissolution). Structural stability is a crucial factor to weigh the effectiveness of battery performance. During the insertion and extraction of Zn^{2+} ions, the vanadium oxide cathode material (e.g. V$_2$O$_5$) undergoes significant volume expansion, which can cause structural collapse and degradation of the material. Vanadium oxides are prone to dissolution in the electrolyte, especially in aqueous systems due to their high solubility in acidic environments. The dissolution of vanadium ions is often driven by electrochemical reactions that occur during the charge/discharge process. The reduction of V^{5+} to V^{4+} or lower oxidation states can lead to the release of vanadium ions into the electrolyte. This dissolution can lead to the loss of the active material and decreased capacity during cycling, further degrading the structural integrity and electrochemical performance of the cathode. This dissolution is particularly pronounced in systems where the electrolyte pH is not well-controlled.[45] Another dissolution example is the vanadium dissolution in VO$_2$ cathodes. This dissolution is exacerbated by structural instability and irreversible phase transformations, which can lead to capacity loss and poor cycling stability.[46] The structural instability can lead to the formation of defects and vacancies, which facilitate the further dissolution of vanadium ions.[45]

2.3.3. Low ion diffusion rate. Low ion diffusion rate would cause problems of slow diffusion kinetics, structural instability, and phase transition effects. The slow Zn^{2+} diffusion kinetics hampers the efficient movement of ions during the electrochemical process. This is due to the intrinsic material structure of vanadium oxide, and the strong electrostatic repulsion between Zn^{2+} and the vanadium-oxygen framework, increasing the resistance to ion movement and slowing down the overall diffusion rate. Some traditional vanadium-based oxides (e.g. V$_2$O$_5$) have limited interlayer spacing, restricting the movement of larger ions like Zn^{2+}. If the Zn^{2+} ions are solvated in aqueous electrolytes, even larger hydrated ions (e.g. Zn (H$_2$O)$_6^{2+}$) form. The small interlayer spacing increases the energy barrier for ion diffusion, resulting in slow kinetics.[47]

The structural instability would degrade the ion diffusion rate. The insertion and extraction of Zn^{2+} ions can cause structural changes and even collapse in the vanadium cathode material during repeated charge/discharge cycles.[48] In some cases, the coexistence of distinct phases (e.g. VO$_2$ (M) and VO$_2$ (R)) can significantly retard the ion diffusion rate. This phenomenon, known as super-susceptibility, can lead to an order of magnitude decrease in effective diffusivity when the material undergoes a first-order phase transition.[49]

2.4. Modification strategies

2.4.1. Guest ion pre-intercalation. In vanadium-based cathode materials for zinc-ion batteries, guest ion pre-intercalation is a technique used to improve these materials' electrochemical performance. The strategy analyses from the two aspects of structural stability and electrochemical properties. Guest ions

function as pillars between the layers of vanadium oxide compounds, preventing the structural collapse during charging and discharging processes.[50] When the layer separation increases, the strong electrostatic interaction between Zn^{2+} and the vanadium oxide skeleton reduces, reducing the diffusion energy barrier of Zn^{2+}.[51] Some guest ions such as Ru^{3+} can increase Gibbs free energy, inhibiting the dissolution of vanadium in the aspect of thermodynamics.[52] From the aspect of electrochemical properties, specific guest ions can be introduced *via* enhancing electron conductivity and increasing active sites. These actions accelerate charge transfer in the process of electrode reaction and induce lattice distortion to expose more reactive oxygen vacancies. In some cases, the co-intercalation layer of several guest ions can produce a synergistic effect to further improve the battery performance, for example, the co-interlayer of Ti^{4+} and K^+.[50]

More examples and studies of guest ion pre-intercalation are shown. Studies have shown that the pre-intercalation of metal cations like Fe^{2+}, Co^{2+}, Ni^{2+}, Mn^{2+}, Zn^{2+}, and Cu^{2+} into V_2O_5 can significantly increase the Zn^{2+} transport rate and cycle stability. Additionally, the introduction of conductive polymers as guest species can improve electron/ion transport rates, resulting in better rate and cycle performances.[18]

2.4.2. Defect engineering. Defect engineering of vanadium cathode materials is a promising approach to enhance their electrochemical performance. This can be achieved by various mechanisms such as improving structural stability, enhancing reaction kinetics, *etc.* By introducing defects such as oxygen vacancies or doping with metal ions (*e.g.* introducing oxygen vacancies into $NH_4V_4O_{10}$), the anion vacancies can reduce the strong electrostatic interaction between the host material and Zn^{2+} ions, thereby alleviating lattice strain during Zn^{2+} insertion/extraction.[53] Similarly, high entropy doping of ions like Na^+, Al^{3+}, Ni^{2+}, NH_4^+, and F^- into the interlayer of $V_2O \cdot 0.48H_2O$ can expand the interlayer spacing, improve electronic/ionic conductivity, and enhance long-term structural stability. Additionally, in some cases, defect engineering enables a self-optimization process during the first charge (*e.g.* Vd-V_2O_3), resulting in a structure where Zn^{2+} can reversibly insert or leave in subsequent cycles.[54]

More examples referring to the self-anchoring effects and synergistic effects have been reported. In self-anchoring, part of the Zn^{2+} ions may anchor in the vanadium vacancies, enhancing the stability of the structure. This self-anchoring effect can prevent the complete extraction of Zn^{2+}, maintaining the structural integrity.[54] Sulphur doping and heterojunction formation are two well-known examples of synergistic effects that can limit the production of inactive byproducts and improve the kinetics and reaction reversibility of the Zn^{2+} and H^+. Heterostructures form by integrating materials with distinct physical and chemical properties, creating synergistic effects and addressing the key challenges of poor charge transfer and limited active surface area. They reduce ion transport barriers, creating low-resistance channels for rapid Zn^{2+} movement.[55] These modifications not only increase the specific capacity and rate performance but also contribute to better cycle stability,

making vanadium-based cathodes more viable for high-performance aqueous zinc-ion batteries.

2.4.3. Macrostructure design. Through a variety of mechanisms, macrostructure design can increase the electrochemical performance of Zn–V static batteries by enhancing the vanadium cathode's conductivity, ion transport, and structural stability. Enhancing the electrode surface area allows the participation of more active sites in the ion exchange process, and optimized pathways reduce the diffusion distance for ions. Thereby, the overall efficiency of the battery improves.

One approach is the use of elemental doping and *in situ* activation. For instance, cadmium doping combined with *in situ* activation has shown to introduce abundant oxygen vacancies and interlayered water, which significantly enhance the electronic and ionic conductivity of vanadium oxides.[56] This results in improved capacity and cycling stability. Another strategy is the pre-intercalation of molecules or ions, such as NH_4^+, which can stabilize the structure *via* hydrogen bonding and facilitate ion diffusion.[57] Structural compositing, such as incorporating conductive polymers or creating oxygen vacancies, is also effective in improving the overall performance of the cathode material. These macro structure design mechanisms collectively contribute to higher capacity, better rate capability, and enhanced cycling stability, making vanadium-based cathodes more suitable for advanced Zn–V static batteries. Additionally, materials such as graphene and other conductive carbon compounds have been utilized to boost the overall conductivity and structural stability of vanadium-based cathodes.[58] The advancement of high-performance vanadium cathode materials for aqueous zinc-ion batteries is significantly supported by these macrostructure design approaches.

2.4.4. Electrolyte modification. Much research has reported various V-based cathodes, which can achieve remarkable capacity (≥ 300 mA h g^{-1}). However, the development of V-based cathodes is limited due to specific pH ranges (between 3.8 and 7.8) of traditional aqueous electrolytes. The electrolyte pH determines the anodic oxidation of vanadium cathode materials and the subsequent zinc storage mechanism.[59] A series of problems regarding the stability, irreversible evolution and dissolution of V-based cathodes are caused by the acidic aqueous electrolytes, and the problem of the precipitation of salt by-products is due to an electrolyte pH imbalance caused by OH^-.[59,60] The continuous release of OH^- from the anode corrosion creates a concentration gradient, causing OH^- ions to migrate to the cathode side. This can lead to the accumulation of byproducts at the cathode surface, which can degrade the capacity of cathode materials. The dissolution problem of V-based cathodes leads to poor battery reversibility and stability in the end.[60]

To solve those problems described above, either direct electrolyte control strategies, such as optimizing the operating potential, controlling the electrolyte pH and using the established pH- and potential-species relationships, or electrolyte modification such as using novel electrolyte additives (*e.g.* $Al_2(SO_4)_3$ or polyethylene glycol combined with a 1 m $Zn(TFSI)_2$ salt (and compared with $Zn(OTf)_2$)) or capping agents (*e.g.* Citric Acid (CA), hexadecyltrimethylammonium bromide (CTAB) and

polyvinyl pyrrolidone (PVP)) could be applied.[60–62] The electrolyte additive, $Al_2(SO_4)_3$, can suppress the H_2O-involved hydrogen evolution, consume the OH^- ions through hydrolysis, and act as a robust pillar.[60] The advanced molecular crowding electrolyte, using polyethylene glycol (PEG) combined with a 1 m Zn $(TFSI)_2$ salt (and compared with Zn $(OTf)_2$), confines water molecules, which reduces water-induced side reactions and leads to an improved electrochemical stability window with an increase of 0.3 V, and enhances ion transport.[61] Capping agents work to form a robust dynamic cathode electrolyte interface, which would isolate free water molecules from the electrodes and prevent the intercalation of hydrated Zn^{2+} ions. The three capping agents undergo different mechanisms to improve the battery performance. Both CA and PVP work through the selective absorption mechanism, differing in targeting different zinc crystal planes, while CTAB works through the surface interaction mechanism.[62]

Both strategies have improved battery performance, where they enhanced the capacity retention (0.2/10 A g^{-1} after 100/4000 cycles for the electrolyte additive, and 91% after over 500 cycles for capping agents). Additionally, $Al_2(SO_4)_3$ has also given batteries an ultralong cycle life (97.6%/98.7%), and the molecular crowding electrolyte has achieved high specific energy ($\sim$190 W h kg^{-1} based on the cathode).[60–62]

3. Zn–V redox flow batteries

3.1. Mechanisms

3.1.1. Reversible redox reactions of Zn and V (two electron or single electron reactions).
In zinc–vanadium redox batteries, carbon felt is used as the positive electrode and a graphite plate is used as the negative electrode. During the charging process, metallic zinc deposits on the electrode of the graphite plate, and the deposited zinc dissolves into the solution when discharged. The reversible redox reactions of Zn and V are fundamental to the battery's operation. The reaction for the zinc anode electrolyte involves the reversible dissolution and plating of zinc: $Zn(s) \leftrightarrow Zn^{2+}(aq) + 2e^-$, with a standard electrode potential of -0.76 V vs. SHE. On the vanadium cathode electrolyte side, the reaction typically involves the V^{5+}/V^{4+} redox couple, which can be represented as $VO_2^+ + H_2O + e^- \leftrightarrow VO^{2+} + 2H^+$, with a standard potential of around +1.00 V vs. SHE. To mitigate the charge difference in the anode and cathode electrolytes, SO_4^{2-} ions in the anode electrolyte diffuse to the intermediate electrolyte via an anion-exchange membrane (AEM), and Na^+ ions in the cathode electrolyte diffuse to the neutral chamber via a cation exchange membrane (CEM). These reactions collectively contribute to the overall battery voltage and energy storage capacity of the battery, as shown in Fig. 12.[63]

3.2. Problems

3.2.1. Poor stability of electrolytes.
The poor stability of electrolytes containing vanadium ions is a significant challenge that hampers the long-term performance and efficiency of these energy storage systems. Vanadium ions, particularly in their
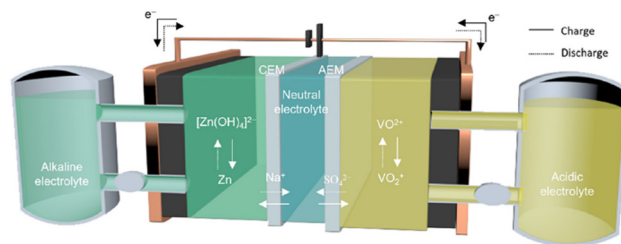

Fig. 12 Schematic of the reversible redox reaction of Zn and V in the Zn–V flow battery.[63] Copyright 2023, the American Chemical Society.

higher oxidation states (V^{5+} and V^{4+}), are prone to precipitation and degradation, especially under the harsh conditions of repeated charging and discharging cycles. For instance, in sulfuric acid-based electrolytes, the solubility of vanadium ions decreases with increasing acid concentration and temperature, leading to the formation of insoluble vanadium oxides such as V_2O_5. This precipitation not only reduces the active material available for redox reactions but also increases the internal resistance of the battery, thereby degrading its performance. Additionally, the electrochemical behaviour of vanadium ions in these electrolytes is often quasi-reversible, resulting in significant overpotentials and reduced charge/discharge efficiencies.[3]

3.2.2. Cross-contamination of vanadium ions.
The cross-contamination of vanadium ions in zinc–vanadium redox batteries presents a significant challenge that adversely affects the functionality and lifespan of these energy storage systems. Within these batteries, vanadium ions exist in various oxidation states (V^{5+}, V^{4+}, V^{3+}, and V^{2+}) in both the catholyte and anolyte; their migration across the ion-exchange membrane can lead to many negative consequences. For instance, the transfer of vanadium ions from the cathode to the anode compartment can result in the generation of undesired vanadium species, which may precipitate and obstruct the membrane and electrodes. This not only diminishes the active material necessary for redox reactions but also raises the internal resistance of the battery, thus reducing its efficiency and lifespan, as shown in Fig. 13.[64] Furthermore, cross-contamination can cause self-discharge and capacity decline, as the redox-active species in the two half-cells gradually become less differentiated.

3.3. Modification strategies

3.3.1. Electrolyte modification.
The V(iv)/V(v) system faces challenges such as poor solubility and stability in sulfuric acid solutions, which hinders the advancement of battery technology. At temperatures exceeding 40 °C, V_2O_5 tends to precipitate, and $[VO_2(H_2O)_3]$ converts to H_3VO_4.[65] This occurs because of the low viscosity in the sulfuric acid solution, which causes structural degradation. In comparison to sulfuric acid solutions acting as the supporting electrolyte, methanesulfonic acid solutions can maintain stability for several months at the optimal operating temperatures of zinc-vanadium batteries, as shown in Fig. 14a–c; furthermore, they exhibit similar viscosity and conductivity to sulfuric acid solutions while being less corrosive.[3]
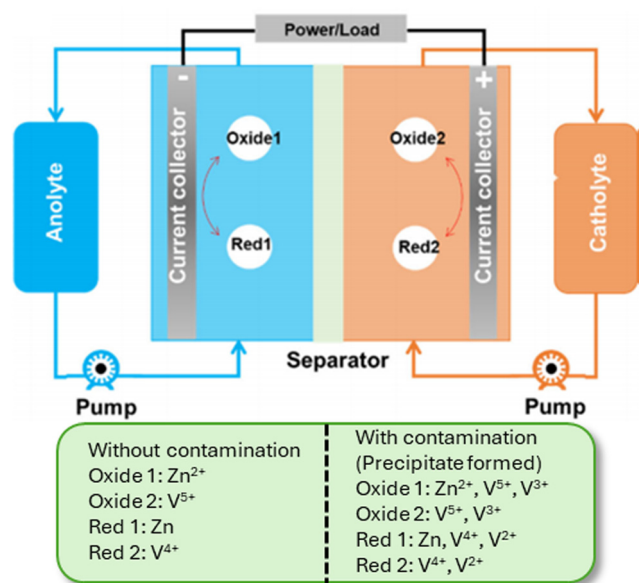
Fig. 13 Schematic of the cross contamination of vanadium ions in the Zn–V flow battery.[64] Reproduced with permission: Copyright 2023, Wiley-VCH GmbH.

MSA offers higher solubility of vanadium ions, better stability, lower viscosity, lower corrosivity, and better electrochemical performance, all of which contribute to improved energy efficiency and longer operational life of the battery, as shown in Fig. 14d–f. These advantages make MSA a promising candidate for enhancing the performance of vanadium redox flow

batteries.[3] Electrolyte modification is a common strategy for aqueous zinc-ion batteries, which is expected to bring novel improvement strategies to Zn–V flow batteries in the future.[66]

3.3.2. Membrane optimization. The membrane plays a crucial role in influencing the performance and stability of the Zn–V hybrid redox flow battery. Two types of membranes have been utilized in this battery: Nafion-117 and a microporous separator. Nafion-117 exhibits high ionic conductivity and excellent selectivity, permitting only certain ions to pass through, which helps maintain electrochemical balance between the anolyte and catholyte while minimizing the crossover of reactive species that can result in self-discharge and decreased efficiency, as shown in Fig. 15a and b. On the other hand, the microporous separator serves as a low-cost option that offers mechanical support and prevents direct contact between the anode and cathode, thus lowering the risk of short-circuiting; however, it encounters issues such as the crossover of V^{4+} ions, leading to capacity loss over multiple charge–discharge cycles, as shown in Fig. 15d. Employing Nafion-117 led to an improved voltage efficiency (84% at 20 mA cm^{-2}), as shown in Fig. 15c. This improvement is due to the membrane's capacity to sustain a stable electrochemical environment and decrease internal resistance, whereas the cell utilizing the microporous separator displayed lower voltage efficiency because of increased internal resistance and ion crossover, which caused a less stable electrochemical environment.[67]

3.3.3. Cathode optimization. The characteristics of the electrode surface play a vital role in influencing the performance of redox flow batteries. Noble metals, carbon materials, and metal oxides have all been utilized to alter these surface
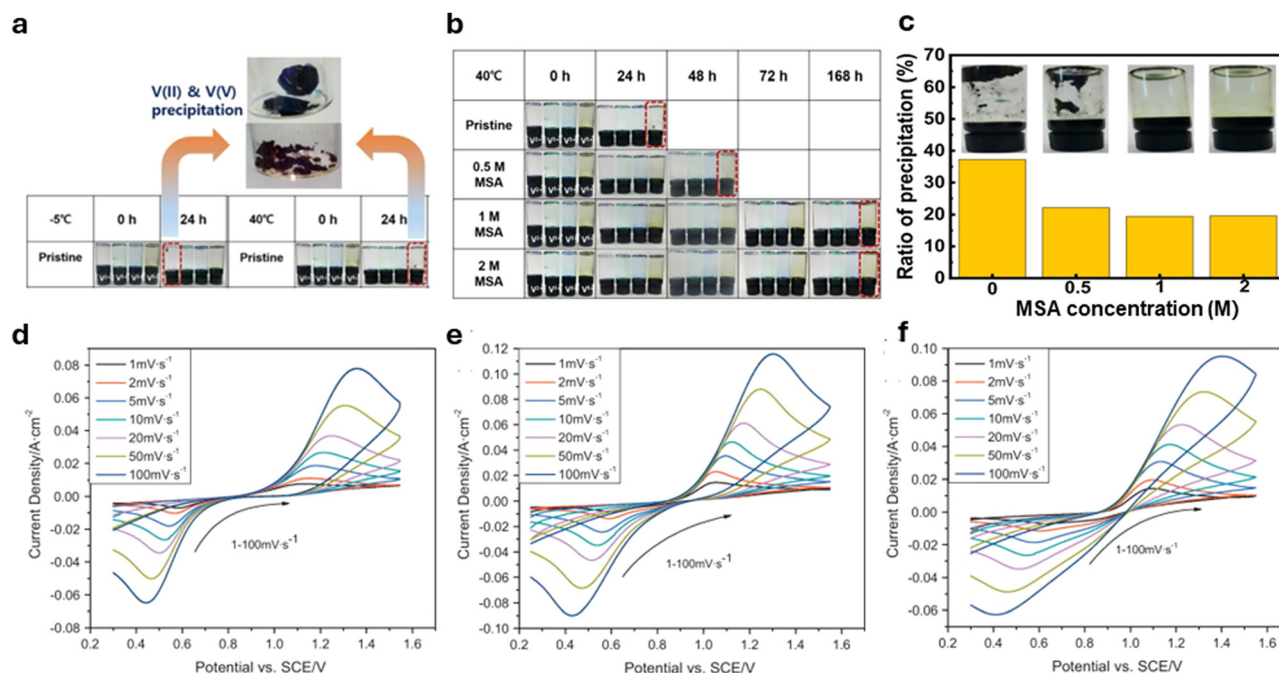

Fig. 14 Schematic of (a) V precipitation without MSA addition at −5 °C and 40 °C at 0 h and 24 h. V precipitation after the stability test of (b) V(II) electrolyte with MSA addition and (c) V(V) electrolyte with MSA addition.[65] Copyright 2021, Elsevier. (d)–(f) Cyclic voltammograms of a stationary Pt electrode in V(V)/V(IV)-MSA solutions with different concentrations of V(V)/V(IV) and scan rates from 1 to 100 mV s^{-1}.[3] Copyright 2012, Elsevier.
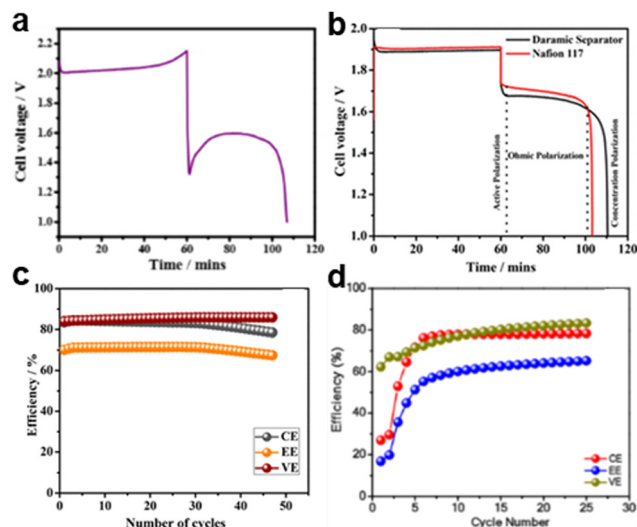
Fig. 15 GCD profiles of (a) Zn–V system and (b) Zn–V flow cell with a Daramic microporous separator and Nafion-117 membrane. Cyclic life of the Zn–V metal hybrid system (c) with a Nafion-117 membrane and (d) with a micro porous separator.[67] Copyright 2019, the American Chemical Society.
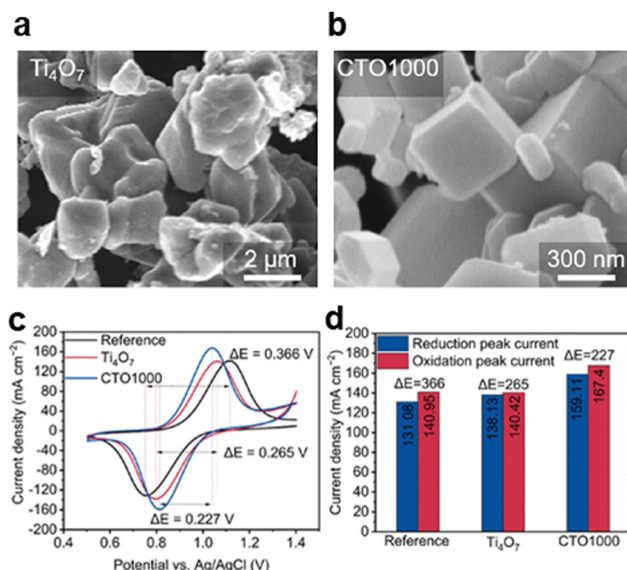

Fig. 16 SEM images of (a) Ti_4O_7 and (b) CTO1000 electrocatalyst. (c) Cyclic voltammograms of pristine CF, Ti_4O_7, and CTO1000 electrodes. (d) Reduction and oxidation peak currents and potential difference of pristine CF, Ti_4O_7, and CTO1000 electrodes.[63] Copyright 2023, the American Chemical Society.

characteristics. However, metal oxides may offer advantages over these three materials because they do not diminish the energy efficiency of batteries like noble metals do. Additionally, unlike carbon-based materials, they do not impede the ion transport of the VO^{2+}/VO_2^+ redox couple within the electrolyte. Among the most frequently used metal oxide compounds for optimizing cathodes are titanium dioxide-based compounds, which demonstrate excellent electrocatalytic performance for the vanadium redox couple, as shown in Fig. 16c.[63]

In 2023, Choi et al. have reported a binary cerium titanium oxide for cathode optimization, and the inversely proportional relationship between the values of oxidation states and the number of formations of oxygen vacancies which function as active sites, which is found by researchers, as shown in Fig. 16a and d. The crystal structure of CTO1000 may affect its catalytic activity through structural defects (e.g. oxygen vacancies), so researchers adjust the crystal structure by controlling the temperature during the synthesis process to enhance the battery performance, as shown in Fig. 16b.[63]

3.4. Advantages of the Zn–V redox flow battery system

Zinc-vanadium redox flow batteries (Zn–V RFBs) exhibit distinct advantages over $Zn–Br_2$ and all-vanadium (All V) systems, particularly in terms of voltage window, power density, and environmental compatibility. While Zn–Br batteries are able to achieve a high open-circuit voltage (2.1 V), their practical current density is significantly limited (<100 mA cm^{-2}) by sluggish Br^-/Br_2 redox kinetics and safety concerns due to toxic bromine volatility, which results in low energy efficiency ($\sim63\%$) and high maintenance costs. On the other hand, Zn–V RFBs combine competitive voltage (1.96 V) with high power density (840 mW cm^{-2}), enabled by the rapid multi-electron reactions of vanadium species (V^{5+}/V^{4+}) and optimized

electrolyte flow rates. Comparing the Zn–V system with all V systems, the anode reaction of the Zn–V system is the reaction of Zn^{2+}/Zn, which has lower potential, leading to a larger voltage window. This is the advantage that all vanadium redox flow batteries do not have. Additionally, Zn–V RFBs leverage zinc's abundance and low toxicity, avoiding the environmental risks of bromine leakage and offering scalable, cost-effective energy storage solutions compared to resource-intensive all V systems. However, the low energy density (16 W h L^{-1}) and short lifespan of Zn–V redox flow batteries need to be overcome to unleash more application potential. These quantitative advantages underline the potential of Zn–V flow batteries as a cost-effective, high-performance alternative for large-scale energy storage, thereby facilitating further development in this field.[64]

4. Conclusion

Zn–V battery systems, encompassing static and flow configurations, have emerged as promising solutions for large-scale
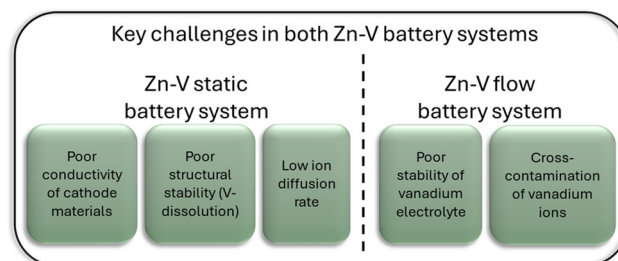

Fig. 17 Schematic of the key challenges of both types of Zn–V batteries.

Table 1 Comparison of Zn–V static battery system and Zn–V flow battery system

Category	Zn–V static system	Zn–V flow system
Mechanism	Zn^{2+} intercalation/extraction H^+/Zn^{2+} co-intercalation H_2O/Zn^{2+} co-intercalation Chemical conversion reactions Other types (substitution/interaction reaction, mixed metal ion mechanism)	Reversible redox reactions of Zn and V, including Zn^{2+}/Zn and the V^{5+}/V^{4+} redox couples
Structures of vanadium cathode materials	Vanadium oxide Vanadium sulphide Vanadium phosphate Vanadium nitride Vanadate	A redox-active vanadium electrolyte (VO_2^+/VO_2^+ species)
Major challenges	Poor conductivity Poor structural stability (V-dissolution) Low ion diffusion rate	Poor electrolyte stability Cross-contamination of vanadium ions
Modification strategies	Guest ion pre-intercalation Defect engineering Macrostructure design Electrolyte modification	Electrolyte modification Membrane optimization Cathode optimization

energy storage, renewable energy integration, and grid stability, leveraging vanadium's multivalent redox chemistry, natural abundance, and environmental compatibility. Vanadium-based cathodes and electrolytes endow these systems with high theoretical capacity, energy density, and safety, driving significant advancement in recent years.

For Zn–V static batteries, progress has been marked by innovations in vanadium-based cathode materials (*e.g.*, oxides, nitrides, and vanadates) with tailored nanostructures, defect engineering, and composite designs to enhance Zn^{2+} storage kinetics and cycling stability. However, challenges persist, including irreversible phase transitions during cycling, vanadium dissolution, and ambiguous energy storage mechanisms—such as debates over Zn^{2+} intercalation *versus* conversion reactions, active phase identification, and byproduct formation—which hinder long-term performance and consensus within the scientific community.

In contrast, Zn–V flow batteries, though still in early-stage research, offer inherent scalability, and adjustable reaction electrode surface area and electrolyte content of storage tanks, attracting growing attention for grid applications. Yet, their development faces hurdles like electrolyte optimization, membrane durability, and cost-effective system integration. The existing knowledge of V cathodes in Zn–V static batteries could be helpful for improvements of Zn–V flow batteries. For example, the electrolyte modification strategy that effectively mitigates vanadium dissolution in the Zn–V static battery system can also be directly used in the flow battery system to solve the problem of ion cross-contamination. In addition, the idea of membrane optimization in Zn–V flow battery systems provides a direction for further battery improvement in static battery systems to weaken the vanadium dissolution and shuttle of Zn–V static batteries (Fig. 17).

Moving forward, resolving mechanistic ambiguities through advanced *in situ*/*operando* characterization, stabilizing vanadium cathodes *via* structural engineering (*e.g.*, pre-intercalation, doping, or protective coatings), and accelerating flow battery innovation through hybrid electrolyte designs and scalable prototypes are critical. Bridging fundamental research with practical engineering will be essential to unlock the full potential of Zn–V batteries, ensuring their viability in the global transition to sustainable energy storage (Table 1).

Author contributions

Y. F. L. wrote and modified the manuscript. J. C. modified the manuscript and gave suggestions and guidance on manuscript improvements. G. J. H. supervised the project and secured the funding. All authors have discussed and agreed to the published version of the manuscript.

Data availability

No primary research results, software or code have been included, and no new data were generated or analysed as part of this review.

Conflicts of interest

The authors declare no conflict of interest.

Acknowledgements

References

1 D. Kundu, B. D. Adams, V. Duffort, S. H. Vajargah and L. F. Nazar, *Nat. Energy*, 2016, **1**, 16119.

2 C. Xu, B. Li, H. Du and F. Kang, *Angew. Chem., Int. Ed.*, 2011, **51**, 933–935.

3 C. Tang and D. Zhou, *Electrochim. Acta*, 2012, **65**, 179–184.

4 L. Shan, J. Zhou, W. Zhang, C. Xia, S. Guo, X. Ma, G. Fang, X. Wu and S. Liang, *Energy Technol.*, 2019, **7**, 1900022.

5 M. Sufyan Javed, H. Lei, Z. Wang, B. Liu, X. Cai and W. Mai, *Nano Energy*, 2020, **70**, 104573.

6 N. Liu, B. Li, Z. He, L. Dai, H. Wang and L. Wang, *J. Energy Chem.*, 2021, **59**, 134–159.

7 F. Wan, L. Zhang, X. Dai, X. Wang, Z. Niu and J. Chen, *Nat. Commun.*, 2018, **9**, 1656.

8 K. Zhu, T. Wu, S. Sun, W. van den Bergh, M. Stefik and K. Huang, *Energy Storage Mater.*, 2020, **29**, 60–70.

9 J. Ding, H. Gao, D. Ji, K. Zhao, S. Wang and F. Cheng, *J. Mater. Chem. A*, 2021, **9**, 5258–5275.

10 E. Roex, F. Boschini, V. Delaval, A. Schrijnemakers, R. Cloots and A. Mahmoud, *J. Electroanal. Chem.*, 2023, **929**, 117133.

11 T. Lv, Y. Peng, G. Zhang, S. Jiang, Z. Yang, S. Yang and H. Pang, *Adv. Sci.*, 2023, **10**, 2206907.

12 Y. Ding, Y. Peng, S. Chen, X. Zhang, Z. Li, L. Zhu, L.-E. Mo and L. Hu, *ACS Appl. Mater. Interfaces*, 2019, **11**, 44109–44117.

13 K. Hu, D. Jin, Y. Zhang, L. Ke, H. Shang, Y. Yan, H. Lin, K. Rui and J. Zhu, *J. Energy Chem.*, 2021, **61**, 594–601.

14 G. Fang, S. Liang, Z. Chen, P. Cui, X. Zheng, B. Lu and X. Lu, *Adv. Funct. Mater.*, 2019, **29**, 1905267.

15 L. Wang, K.-W. Huang, J. Chen and J. Zheng, *Sci. Adv.*, 2019, **5**, eaax4279.

16 M. Chen, S.-C. Zhang, Z.-G. Zou, S.-L. Zhong, W.-Q. Ling, J. Geng, F.-A. Liang, X.-X. Peng, Y. Gao and F.-G. Yu, *Rare Met.*, 2023, **42**, 2868–2905.

17 L. Shan, Y. Wang, S. Liang, B. Tang, Y. Yang, Z. Wang, B. Lu and J. Zhou, *InfoMat*, 2021, **3**, 1028–1036.

18 T. Zhou and G. Gao, *Nano Energy*, 2024, **127**, 109691.

19 S. Liu, L. Kang, J. M. Kim, Y. T. Chun, J. Zhang and S. C. Jun, *Adv. Energy Mater.*, 2020, **10**, 2000477.

20 P. Hu, M. Yan, T. Zhu, X. Wang, X. Wei, J. Li, L. Zhou, Z. Li, L. Chen and L. Mai, *ACS Appl. Mater. Interfaces*, 2017, **9**, 42717–42722.

21 D. Chen, X. Rui, Q. Zhang, H. Geng, L. Gan, W. Zhang, C. Li, S. Huang and Y. Yu, *Nano Energy*, 2019, **60**, 171–178.

22 S. Lee, I. N. Ivanov, J. K. Keum and H. N. Lee, *Sci. Rep.*, 2016, **6**, 19621.

23 X. Xu, F. Xiong, J. Meng, C. Wang, C. Niu, Q. An and L. Mai, *Adv. Funct. Mater.*, 2020, **30**, 1904398.

24 L. Chen, Y. Ruan, G. Zhang, Q. Wei, Y. Jiang, T. Xiong, P. He, W. Yang, M. Yan, Q. An and L. Mai, *Chem. Mater.*, 2019, **31**, 699–706.

25 H. Chen, J. Huang, S. Tian, L. Liu, T. Qin, L. Song, Y. Liu, Y. Zhang, X. Wu, S. Lei and S. Peng, *Adv. Sci.*, 2021, **8**, 2004924.

26 C. Liu, Z. G. Neale, J. Zheng, X. Jia, J. Huang, M. Yan, M. Tian, M. Wang, J. Yang and G. Cao, *Energy Environ. Sci.*, 2019, **12**, 2273–2285.

27 J. Chen, Y. Liu, B. Xiao, J. Huang, H. Chen, K. Zhu, J. Zhang, G. Cao, G. He, J. Ma and S. Peng, *Angew. Chem., Int. Ed.*, 2024, **63**, e202408667.

28 Y. Zhang, A. Chen and J. Sun, *J. Energy Chem.*, 2021, **54**, 655–667.

29 C. S. Rout, B.-H. Kim, X. Xu, J. Yang, H. Y. Jeong, D. Odkhuu, N. Park, J. Cho and H. S. Shin, *J. Am. Chem. Soc.*, 2013, **135**, 8720–8725.

30 P. He, M. Yan, G. Zhang, R. Sun, L. Chen, Q. An and L. Mai, *Adv. Energy Mater.*, 2017, **7**, 1601920.

31 K. Chen, X. Li, J. Zang, Z. Zhang, Y. Wang, Q. Lou, Y. Bai, J. Fu, C. Zhuang, Y. Zhang, L. Zhang, S. Dai and C. Shan, *Nanoscale*, 2021, **13**, 12370–12378.

32 R. Gautier, R. Gautier, O. Hernandez, N. Audebrand, T. Bataille, C. Roiland, E. Elkaïm, L. Le Pollès, E. Furet and E. L. Fur, *Dalton Trans.*, 2013, **42**, 8124.

33 Y. Li, W. Li, H. Chen, Z. Liu, X. Li and D. Zhou, *J. Electroanal. Chem.*, 2024, **974**, 118755.

34 J. Chen, K. Guo, T. Ren, G. Feng, W. Guo and F. Bao, *J. Power Sources*, 2024, **626**, 235751.

35 Y. Niu, W. Xu, Y. Ma, Y. Gao, X. Li, L. Li and L. Zhi, *Nanoscale*, 2022, **14**, 7607–7612.

36 H. Wang, W. Hou, X. Wang, X. Xie, H. Peng, G. Ma, L. Zhu and Y. Xu, *Chem. - Eur. J.*, 2025, **31**, e202403903.

37 H. Chen, Z. Yang, J. Wu, Y. Rong and L. Deng, *J. Power Sources*, 2021, **507**, 230286.

38 X.-F. Ma, H.-Y. Li, W. Ren, D. Gao, F. Chen, J. Diao, B. Xie, G. Huang, J. Wang and F. Pan, *J. Mater. Sci. Technol.*, 2023, **153**, 56–74.

39 C. Xia, J. Guo, Y. Lei, H. Liang, C. Zhao and H. N. Alshareef, *Adv. Mater.*, 2017, **30**, 1705580.

40 M. Wang, G. Zhao, X. Yu, X. Bai, A. Chen, C. Zhao, P. Lyu and N. Zhang, *Nano Energy*, 2023, **110**, 108336.

41 L. Chen, H. Wu, H. Wang, L. Chen, X. Pu and Z. Chen, *Electrochim. Acta*, 2019, **307**, 224–231.

42 C. R. Tang, G. Singh, L. M. Housel, S. J. Kim, C. D. Quilty, Y. Zhu, L. Wang, K. J. Takeuchi, E. S. Takeuchi and A. C. Marschilok, *Phys. Chem. Chem. Phys.*, 2021, **23**, 8607–8617.

43 X. Chen, H. Zhang, J.-H. Liu, Y. Gao, X. Cao, C. Zhan, Y. Wang, S. Wang, S.-L. Chou, S.-X. Dou and D. Cao, *Energy Storage Mater.*, 2022, **50**, 21–46.

44 X. Ding, J. Le, Y. Yang, L. Liu, Y. Shao, Y. Xiao, Y. Li and L. Han, *Energy Storage Mater.*, 2025, **76**, 104098.

45 X. Ren, M. Sun, Z. Gan, Y. Sun, N. Wang, L. Hu, Z. Yan, C. Jia and Z. Li, *Chem. Eng. J.*, 2024, **494**, 152994.

46 Y. D. Luna, Z. Mohamed, A. Dawoud and N. Bensalah, *RSC Adv.*, 2024, **14**, 39193–39203.

47 D. Sun, M. Zhang, W. Wan, Y. Cao and H. Chai, *J. Energy Storage*, 2023, **73**, 109236.

48 S. Bai, Z. Wu, X. Zhang, J. Qiu, J. Chen, Z. Liu and Y. Zhang, *Chem. Eng. J.*, 2024, **500**, 157281.

49 Y. Cai, Z. Wang, J. Wan, J. Li, R. Guo, J. W. Ager, A. Javey, H. Zheng, J. Jiang and J. Wu, *Nat. Commun.*, 2024, **15**, 5814.

50 B. Hu, X. Yang, D. Li, L. Luo, J. Jiang, T. Du, H. Pu, G. Ma, B. Xiang and Z. Li, *J. Alloys Compd.*, 2024, **1008**, 176801.

51 T. Zhou and G. Gao, *J. Energy Storage*, 2024, **84**, 110808.

52 Z. Chen, H. Liu, S. Fan, Q. Zhang, C. Yuan, W. Peng, Y. Li and X. Fan, *Adv. Energy Mater.*, 2024, **14**, 2400977.

53 J. Gao, C. Cheng, L. Ding, G. Liu, T. Yan and L. Zhang, *Chem. Eng. J.*, 2022, **450**, 138367.

54 K. Zhu, S. Wei, H. Shou, F. Shen, S. Chen, P. Zhang, C. Wang, Y. Cao, X. Guo, M. Luo, H. Zhang, B. Ye, X. Wu, L. He and S. Li, *Nat. Commun.*, 2021, **12**, 6878.

55 S. Hou, X. Chen, G. He, X. Peng, J. Wang, C. Huang, H. Liu, T. Liu, X. Wang, S. Hou and L. Zhao, *J. Mater. Chem. A*, 2025, **13**, 1240–1248.

56 T. Chen, Q. Wu, L. Lang, Z. Chen, G. Luo, L. Hu, G. Liu and W. Chen, *Chem. Eng. J.*, 2024, **499**, 156295.

57 K. Fang, H. Zhang, P. Chen, H.-Y. Zhang, Z. Wei, L. Ding, X.-A. Ye, J. Liu, Y.-L. Liu, G.-G. Wang and H. Y. Yang, *Chem. Eng. J.*, 2024, **496**, 153736.

58 T.-H. Wu, T.-K. Li and L.-J. Guo, *J. Power Sources*, 2024, **623**, 235503.

59 Y. Li, H. Ba, Z. Wang, S. Wu, Y. Shang, S. Huang and H. Y. Yang, *Mater. Today Energy*, 2023, **39**, 101460.

60 D. Liu, Z. Zhang, Y. Zhang, M. Ye, S. Huang, S. You, Z. Du, J. He, Z. Wen, Y. Tang, X. Liu and C. C. Li, *Angew. Chem.*, 2023, **135**, e202215385.

61 D. E. Ciurduc, C. de la Cruz, N. Patil, A. Mavrandonakis and R. Marcilla, *Mater. Today Energy*, 2023, **36**, 101339.

62 R. Chen, Y. Zhong, P. Jiang, H. Tang, F. Guo, Y. Dai, J. Chen, J. Wang, J. Liu, S. Wei, W. Zhang, W. Zong, F. Zhao, J. Zhang, Z. Guo, X. Wang and G. He, *Adv. Mater.*, 2025, 2412790, DOI: **10.1002/adma.202412790.**

63 J. Choi, J. Park, J. Park, M. Kim, S. Lee, C. R. Cho, J. H. Lee, Y. Park, M. G. Kim, J. Choi, J.-W. Park and M. Park, *ACS Appl. Mater. Interfaces*, 2023, **15**, 55692–55702.

64 Q. Zhao, G. Yin, Y. Liu, R. Tang, X. Wu and X. Zeng, *Carbon Neutralization*, 2023, **2**, 90–114.

65 G. Kim, Y. Kim, T. Yim and K. Kwon, *J. Ind. Eng. Chem.*, 2021, **99**, 326–333.

66 W. Zong, J. Li, C. Zhang, Y. Dai, Y. Ouyang, L. Zhang, J. Li, W. Zhang, R. Chen, H. Dong, X. Gao, J. Zhu, I. P. Parkin, P. R. Shearing, F. Lai, K. Amine, T. Liu and G. He, *J. Am. Chem. Soc.*, 2024, **146**, 21377–21388.

67 M. Ulaganathan, S. Suresh, K. Mariyappan, P. Periasamy and R. Pitchai, *ACS Sustainable Chem. Eng.*, 2019, **7**, 6053–6060.